Chinese Chemical Letters 34 (2023) 107275

Contents lists available at ScienceDirect

Chinese Chemical Letters

journal homepage: www.elsevier.com/locate/cclet

Boron: A key functional component for designing high-performance heterogeneous catalysts

Meihong Fan[a], Xiao Liang[b], Qiuju Li[c], Lili Cui[a], Xingquan He[a,*], Xiaoxin Zou[b,*]

[a] School of Chemistry and Environmental Engineering, Changchun University of Science and Technology, Changchun 130022, China
[b] State Key Laboratory of Inorganic Synthesis and Preparative Chemistry, College of Chemistry, Jilin University, Changchun 130012, China
[c] Department of Chemistry, College of Basic Medicine, Third Military Medical University (Army Medical University), Chongqing 400038, China

ARTICLE INFO

Article history:
Received 30 December 2021
Revised 22 January 2022
Accepted 27 February 2022
Available online 4 March 2022

Keywords:
Boron
Heterogeneous catalysis
Active site
Electronic structure
Structure-activity relationship

ABSTRACT

Heterogeneous catalysis is a vivid branch of traditional catalysis field, with the advantage of high efficiency and being easily separated from reactants and products after reaction, and have received widespread attentions in large-scale industrial production, especially in the field of energy utilization. Boron has been found to be a key functional component for designing high-performance heterogeneous catalysts. In this review, we cover and categorize the past and recent progress in boron-containing materials and their applications in heterogeneous catalysis particularly in energy-related fields. The fundamental roles of boron components in the emerging heterogeneous catalysis of construction, regulation and stabilization of active phases/sites are highlighted, with the emphasis on how they regulating structural and electronic properties of host materials. We then categorize boron-containing catalysts into six kinds mainly including intermetallic boride catalysts, metal boride-derived catalysts, boron-doped catalysts, metal boride-decorated catalysts, boron-containing compounds as catalyst supports, and single-boron-site catalysts, as well as try to establish structure-catalytic activity relationship. The catalytic applications of these six boron-containing catalysts are discussed separately, focusing on the energy-related reactions such as hydrogen evolution reaction (HER), oxygen evolution reaction (OER), oxygen reduction reaction (ORR), carbon dioxide reduction reaction (CO_2RR) and nitrogen reduction reaction (NRR). Finally, the opportunities and challenges related to boron-containing compounds in the field of catalysis are prospected.

1. Introduction

Boron, the fifth element in the periodic table, neighbores with carbon but displays quite different physical and chemical properties with it. Boron presents chemical properties similar to Si, Ge and As, which are also located on the boundary line between metals and nonmetals and are all well-known as metalloid. Unlike other elements in IIIA group, boron with the electronic structure of $1s^2 2s^2 2p^1$ has unique medium electronegativity and electron deficiency characteristics [1,2]. Often it utilizes all three of its valence electrons to form covalent compounds in the form of BR_3 (R= hydroxyl, alkoxyl, alkyl, halo, *etc.*) with sp^2 hybridized orbitals in many solid-state boron-containing materials [3,4]. The earliest report on elemental boron was made by Humphry Davy in a lecture in the Royal Institution in London in 1807 [5,6]. He shared his new findings in experiment that "dark combustibles" matter would be obtained by the reduction of wet boric acid with electric current. This is the primary understanding of element B. Naturally occurring boron is widely distributed in the environment with a crustal abundance of *ca.* 0.001% [7,8]. Although relatively uncommon element as it belongs to, the distribution of element B is universal as it exists in all natural waters, like freshwater lakes and rivers, soils and borate ores [9–11]. Meanwhile, boron is also a key element in the formation of RNA and plant cell wall and has been found to play important roles in the regulation of plant enzymes in nitrogen fixation reaction. Boron was used in glass and detergent production as early as 30 years ago. Nowadays it has been widely employed in drug synthesis, organic light-emitting diode (OLED) screen and solar cell preparation [12,13].

Dominated by the medium electronegativity and electron deficient character of boron, the bonding states of boron element are unusual and variable in all of its compounds [4,14]. In organic boron chemistry, boron center has always been considered as electrophilic reagent until the synthesis of boryllithium salt to serve as a strong nucleophilic reagent in 2006 [15]. This finding

* Corresponding authors.
E-mail addresses: hexingquan@hotmail.com (X. He), xxzou@jlu.edu.cn (X. Zou).

https://doi.org/10.1016/j.cclet.2022.02.080
1001-8417/

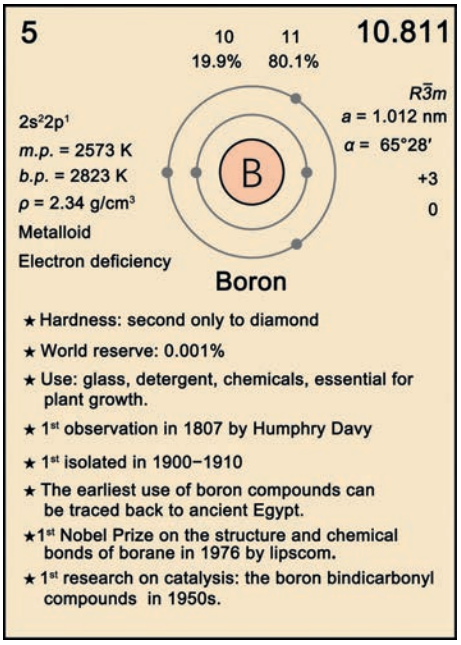

Fig. 1. Summary of physicochemical parameters and significant event related to element boron.

flipped the 100 years history of boron chemistry upside down. Boron even shows the characteristics of transition metal elements and can effectively activate nitrogen in the boron-containing carbonyl compounds synthesized in 2018 [16]. In terms of inorganic boron chemistry, boron can bond with almost all metal elements to form metal borides, owning vast and complex chemical bonding forms, including metallic metal-metal bond, metallic metal-boron bond, ionic metal-boron bond, and covalent boron-boron bond. Metal borides also show a variety of crystalline forms, up to more than 150 kinds of crystal structures [17–19]. The diversity of element composition, chemical bonding and crystal structure endows metal borides with significant bulk phase properties [20,21]. For example, the superconductivity of MgB_2 and the superhardness effect of ReB_2 are research hotspots in recent years. $Nd_2Fe_{14}B$ is an important rare earth permanent magnet material. TiB_2 is applied to the manufacture of crucible and electrolytic cell electrodes as anti-corrosion materials [22–26]. Metal hydrides, particularly sodium borohydride, have emerged as preeminent reducing agent that was capable of reducing most functional groups in organic chemistry [27]. Efforts in scientific research promote rapid development of boron chemistry, and eventually research in the field of boron awarded the Nobel Prize. For example, William N. Lipscomb won the Nobel Prize in 1976 for his research on the structure and chemical bonds of borane [28]. At the same time, Brown discovered a brand-new boron-containing compound, organoborane, an important reagent in organic synthesis, and was rewarded the Nobel Prize [29]. Suzuki shared the prize in 2010 for his finding of palladium catalyzed cross coupling reaction for organic synthesis by using boron as a new universal connector for carbon-carbon bond formation [30].

Application of boron-containing compound in catalysis can be dated up to1950s [17] and important information related to boron element is summarized in Fig. 1. Nickel-based boride was found to be a more efficient catalyst for the hydrogenation reaction than the famous Raney nickel catalyst. Doping of small amount of boron promoter in the crystal lattice of silver electrode was found to be effective in improvement of the effectiveness of silver as an oxidant catalyst in fuel cells [27,31]. However, in most cases virtually nothing is known about mechanism or reactive intermediates, as well as progress on metal borides as catalytic materials has not been much developed [32,33]. Because most metal borides involved in catalytic reactions are amorphous borides or boron doped alloys, having merits of uncertainty of boron content, randomness of boron distribution and the limitation of metal elements involved. Moreover, limitations on the backward technical means at that time also hindered research on boron containing catalysts [4]. There are two main difficulties: (1) It is hard to synthesize metal boride with definite crystal structure [34,35]; and (2) electronic interaction between metal and boron atoms on catalytic properties of material surface is poorly understood. However, things are different today. Renaissance in boron chemistry is all the more remarkable in rational design of boride catalysts and understanding on structure-activity relationships, as well as their exciting catalytic properties are the primary driving force [36]. That is benefiting from the advancement of characterization technology which can analyze crystal structure and bonding style directly, theoretical calculations can rapidly forecast novel catalysts and reveal the roles of B in promoting catalytic performance. Especially in the recent five years, catalytic applications of B-containing compound in energy-related fields, such as the hydrogen evolution reaction (HER), oxygen reduction reaction (ORR), N_2 reduction reaction (NRR), and CO_2 reduction reaction (CO_2RR) have attracted continuous attention and many novel B-containing catalysts were reported [37–40].

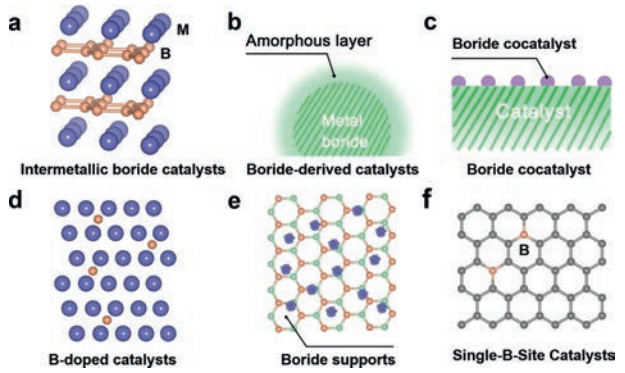

Fig. 2. Schematic illustration of the six types of boron-containing catalysts.

In this review, we summarize recent investigations on the use of boron in designing high-performance heterogeneous catalysts (Fig. 2). We first briefly summarize three important functions of B in the boron-containing catalysts, including constructing active phase, regulating active species and stabilizing active sites. After that, we give a thorough classification of catalysts that element boron involved in discussing their bond styles and surface structures as well as the understanding process on them. In this section, we investigate the role B plays in electronic structure and surface adsorption capacity modulation for many key heterogeneous catalytic reactions in energy conversion fields. Finally, we discuss the future directions and challenges on the development of boron-based catalysts.

2. Fundamental roles of boron components in catalysis

Boron-containing materials are widely used in the field of energy conversion and catalysis. In this section, the role of boron in the material was summarized and reviewed on the main results obtained so far in the literature.

2.1. Direct construction of catalytic active phases

Boron can combine with almost all metallic or metalloid elements to form intermetallic compounds, whose crystal structures

are totally different from that of the constituent metal and boron element [41,42]. Intermetallic borides have various compositions and stoichiometries varying from M_4B, M_3B, M_2B to MB_4, MB_6 and MB_{12} [43,44]. They have subunits with isolated boron atoms, single and double chains of boron and even three-dimensional array in the metal atom lattice [27]. The electron-deficient merit and abundant bonding modes of boron have endowed intermetallic borides developed into a big family [45,46]. These intermetallic borides can be used as catalysts to offer efficient active sites with multifarious configurations toward numerous catalytic reactions. For example, intermetallic borides such as RuB_2, Pd_2B, RhB, RuB were found to be efficient electrocatalysts with Pt-like activities for HER [47–51]. Their electrocatalytic activities are much higher than corresponding pure metal samples. Moreover, some precious-metal-free intermetallic borides (*e.g.*, MoB_2, WB_2) could exhibit high activities toward HER [37,52]. Two dimensional borophene monolayers existed in MoB_2 was believed to endow borides high electrical conductivity and activity due to the graphene like structures of the subunits [53,54]. Chen *et al.* found that α-MoB_2 comprising borophene subunits can deliver large current densities in the order of 1000 mA/cm^2, demonstrating excellent catalytic stability during HER [37]. Intermetallic borides are also helpful to construct catalytic active phases for some reactions like NRR, OER and ORR. The Liu Group theoretically investigated several molybdenum boride catalysts (Mo_2B, α-MoB and MoB_2), and identified Mo_2B phase containing isolated B sites to be potential candidate for NRR [55]. The M_2B (M = Fe, Co, Ni) on metal sheets were highly active phases to catalyze OER [56]. Sato's theoretical modelling revealed that B-doped Pd (Pd-B) weakens the absorption of ORR intermediates with nearly optimal binding energy by lowering the barrier associated with O_2 dissociation, suggesting that Pd-B should be highly active for ORR [57].

The stability of intermetallic boride catalysts should also be considered in catalytic process. For example, in intermetallic Pd-B compounds, boron atoms would leach out from its position during electro-catalyzing HER, leading to inactivation of the material [58,59]. The leaching amount of B was found to be dependent on the ordering of interstitial boron atom. Boron leached out more in the disordered structure while less in an ordered structure. That is to say, ordering of interstitial boron atoms helped keep structural and catalytic stability of borides [49]. Moreover, in some oxidation reactions like OER, intermetallic borides would experience structural evolution [60,61]. For example, metal boride layers on metal sheets were found to transform into metaborate modified metal hydroxyl oxides, serving as the real catalytic active phase [56,62,63]. The mechanism of boron leaching out and structural evolution of intermetallic borides during some catalytic process still maintain poorly understood and require continuous research efforts.

2.2. Regulation of the properties of catalytic active phases

In addition to directly construct catalytic active phase, boron or boron species can regulate the properties of catalysts through doping and surface modification. Doping boron atom into the metal lattices of catalysts offers the possibility to tune the chemistry of the host materials. As a light element with small atomic radius, boron has long been known that it can penetrate into the interstitial sites of noble metal lattices during synthesis and/or catalysis easily [64,65]. Some studies have observed that the solubility, distribution and ordering of light elements in metal interstitials will affect the lattice parameters, structural stability and other bulk properties of host metal materials [66–68], and some studies have observed the influence on catalytic performance [69–71]. Introducing boron into metal lattices can trigger some interesting electrochemical behaviors and boost the catalytic performances in

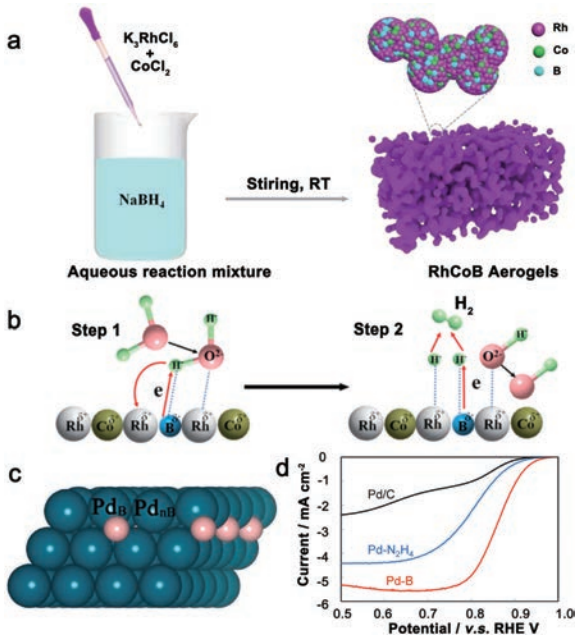

Fig. 3. (a) Schematic illustration of the synthesis process of the RhCoB aerogels. (b) Schematic HER electrocatalysis process on RhCoB aerogels in an alkaline electrolyte. Reproduced with permission [51]. Copyright 2020, Royal Society of Chemistry. (c) B-doped Pd surface model. (d) Electrochemical performances of ORR catalysts, Pd–B, Pd–N_2H_4 and Pd/C nanoparticles. Reproduced with permission [57]. Copyright 2016, Wiley-VCH.

several processes. Rh and transition metal M (M = Co, Ni and Fe) spongy aerogels incorporated with boron atoms can act as highly efficient hydrogen evolution electrocatalyst, as illustrated in Figs. 3a and b [51]. Interstitial boron modification of palladium nanoparticles (Figs. 3c and d) was found to lead a strong host-guest electronic interaction, which can catalyze hydrogenation process with enhanced selectivity [57]. In another work, boron doping into palladium catalyst showed excellent catalytic performance towards ORR by weakening the absorption of oxygen-containing intermediates and hence lowering the reaction barrier [38]. Though these metal-B alloys exhibited improved catalytic activity/selectivity than their metallic counterparts, there is still a lack of understanding on the structure-activity relationship due to the small size, random distribution and low content of boron in metal lattices. Accurate synthesis of alloys with well-defined boron content and ordering may be the future research hotpot.

In addition to alloy catalysts, boron doping also has the effect of adjusting the catalytic active phase for some metal anchored carbon-based catalytic materials. Boron doping was reported to trigger synergetic effect of electronic interaction between dopant elements and parent metals, which in turn promote the catalytic efficiency by acting as bases to promote the discharge step and/or modifying the hydrogen adsorption properties on active sites. Tsiakaras *et al.* reported the one-pot synthesis of boron-doped RhFe alloy with diameter ranging from 1 nm to 5 nm, which is uniformly distributed on the carbon support. The boron-doped RhFe alloy with molar ratio Rh:Fe = 2:1 (named BRF21) showed the most excellent catalytic performance for HER that it needed near zero onset potential and 25 mV to deliver a current density of 10 mA/cm^2. The remarkable property was originated from boron doping and alloying, which would compress the lattice parameter of BRF21 and change the overlapping rate of neighboring atoms' electron orbitals. These changes may modify the energy of electron transfer and increase the d-band density of electron at Fermi level and improve the catalytic activity [72].

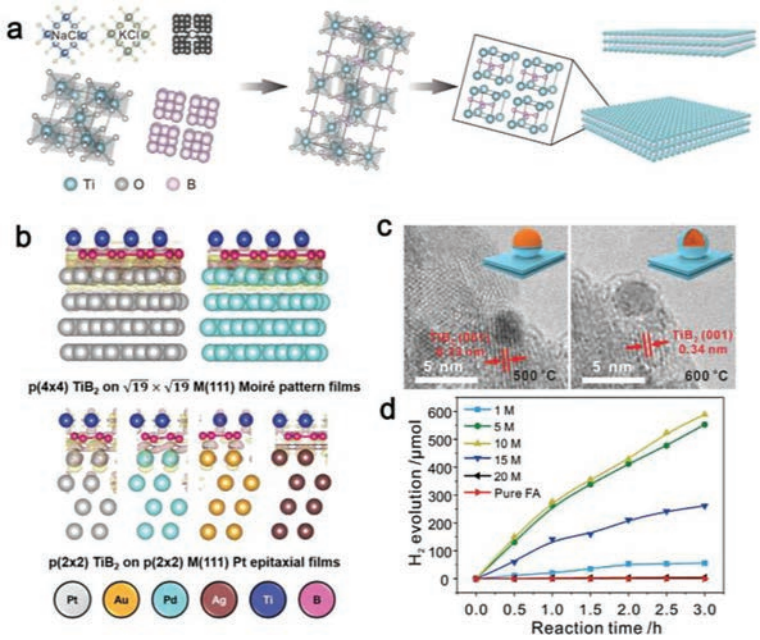

Fig. 4. (a) Schematic illustration of the molten salt-assisted borothermal reduction process to prepare TiB_2. (b) Charge density difference plots representing charge transfer induced by TiB_2 films on the metal. (c) HRTEM images of Pt/TiB_2-500 and Pt/TiB_2-600. (d) H_2 evolution as a function of reaction time for the dehydrogenation of different concentration of formic acid (FA) catalyzed by Pt/TiB_2-600 (20 mg, Pt loading amount is 12.0 wt%) in N_2 atmosphere at 25 °C. Reproduced with permission [75]. Copyright 2021, Wiley-VCH.

Moreover, the B species can also be used as cocatalysts to decorate the surface of photo(electo)catalysts and modify the chemical properties of parent materials. Recombination of photoinduced electrons and holes is the main problem in photo(electo)catalysis. Metal borides decorating on the surface as cocatalysts can inhibite the recombination and thus improve catalytic efficiency [73]. The most convincing reason is that the energy band of some boron-containing cocatalyst matches with that of semiconducting photocatalysts, thus facilitating electron-holes seperation and optimizing catalytic performance. Metals borides are emphasized as cocatalysts for efficient photocatalytic HER due to their excellent conductivity and kinetics. CoB nanosheets and FeB nanoplates were reported to hydrothermally modify WO_3 thin films and improve water oxidation catalytic performance. This is due to the synergetic effects produced by coupling WO_3 with *in situ* formed core-shell nanostructure [74].

2.3. Stabilization of catalytic active sites as supports

Developing advanced supporting materials to load metal catalysts with good dispersion can expose more accessible active sites, which results in increased mass activity and improved stability. The strong metal-support interactions are key concept in heterogeneous catalysis and often play an important role in the preparation of stable noble metal nanocatalysts. The synthesis of TiB_2 nanosheets was illustrated in Fig. 4a [75]. Ideal supporting material should not only protect metal centers from aggregation but also regulate the electronic structure of the host metals through the strong metal-support interactions, providing opportunity to change its structure, surface composition and optimize the catalytic activities synergistically (Fig. 4b) [75]. The development of two-dimensional layered boron nitride materials as supports in heterogeneous catalysis has been a matter of fact for its low density, high thermal conductivity, electrical insulation, superb oxidation resistance, excellent inertness, and low friction coefficient. Monolayers of hexagonal boron nitride (h-BN) have been successfully used as dielectric substrates in graphene electronic devices, thermally robust catalytic, sensing substrates and chemically inert superhydrophobic films, *etc.* [76].

Metal-support interactions in these nanomaterials have a substantial influence on catalysis [77]. Esrafili *et al.* also claimed that Pd loaded on the boron-vacancy defect of BN nanosheet preferably to adsorb CO rather than O_2 energetically. A termolecular Eley-Rideal (TER) mechanism was proposed for its small activation energies. B vacancy defect induced strong interaction between the Pd and undercoordinated nitrogen atoms as well as large electron density loss over the Pd atom, leading to a high energy barrier for surface Pd atom diffusion, that is high stability of Pd atom over the B-vacancy defect of h-BN sheet [78]. Joshi *et al.* reported the synthesis of iridium oxide (IrO_2) nanoparticles supported on boron and nitrogen co-doped reduced graphene oxide (BN-rGO) by simple pyrolysis and hydrothermal methods [79]. They found that the B-N, B-C, and N-C functional groups in the hybrid can support and stabilize the IrO_2 catalyst nanoparticles. In particular, the chemically and electrochemically stable B-N bond would cause the electronic state of IrO_2 to change, so that the composite exhibited excellent OER catalytic activity and stability. Besides being used as substrates, boron in boron nitride was found to participate in the catalyst synthesis as boron source to diffuse into the palladium catalyst lattice. The dopant modified palladium nanoparticles, gave unparalleled performance in the continuous semi-hydrogenation of alkynes [80].

Besides loading noble metal catalysts on the well-known metal-free boron nitride layered substrate, recent studies have also reported on employing transition metal borides layers as substrates for noble metal catalysts dispersion for their metal-like electronic conductivity, high melting point, exceptional physical hardness and low work function. Liu and colleagues reported TiB_2 supportted Pt reconstructed interface (Figs. 4c and d) were highly efficient in catalyzing the dehydrogenation of formic acid at room temperature. Strong metal-support interactions existed on the interface of Pt/TiB_2, which promotes catalytic activity and stability simultaneously. The fabrication of porous borides with large specific surface area as the substrate for electrocatalyst maybe a promising method for stabilizing catalytic active sites, especially consid-

ering the high conductivity and corrosion resistance of many transition metal borides. One should keep in mind that amorphous boron oxide layer may be formed on the surface of transition metal borides, which is unnegligible for loading method and cataytic performance.

3. Boron-containing heterogeneous catalysts

Along with the inorganic boron chemistry renaissance, numerous boron-containing compounds have been emerging as promising inorganic functional materials like catalysts. They possess excellent catalytic activity, stability and selectivity which depends heavily on the flexibility of boron element on constructing, regulating and stabilizing active sites. Considering the role B plays in hetero-catalysis, boron-based catalysts can be divided mainly into six categories. Boron-based catalysts for constructing catalytic active phases include (1) intermetallic boride catalysts; (2) metal boride-derived catalysts; and (3) single-boron-site catalysts. In addition, boron-based catalysts for regulating catalytic active phases include (4) metal boride-decorated catalysts; and (5) boron-doped catalysts. And boron-based catalysts for stabilizing catalytic active phases include (6) boron-containing compounds as catalyst supports.

3.1. Intermetallic boride catalysts

Owing to the electron-deficient properties, and moderate electronegativity of boron, intermetallic borides exhibit very diverse compound types and bonding structures. Currently, more than 200 binary and 800 ternary intermetallic borides have been discovered, covering 150 different crystal structure types. These crystal structures mainly include M-M/M-B metallic bonds, M-B ionic bonds and B-B covalent bonds. The B-B covalent bonds also contain abundant structural forms, ranging from 1D boron chains to 2D boron layers to 3D boron frameworks [81,82]. Previous articles have reviewed the structure and synthesis methods of metal borides, so here we mainly discuss the catalytic application of intermetallic borides especially in fields of energy conversion.

In 2012, the commercially available molybdenum boride (MoB) was first reported to be an active HER electrocatalyst by Park *et al.* [83]. This work encouraged research on the Mo-B intermetallics toward HER. Subsequently, the Zou group systematically investigated the HER catalytic activities of four Mo-B phases with different structures, including α-MoB_2, β-MoB_2, MoB and Mo_2B. Among them, α-MoB_2 with borophene subunits (Figs. 5a–c) exhibited significantly higher activity than Pt/C in a wide current density range above $\sim$250 mA/cm^2 [37]. Density functional theory (DFT) calculations indicated that such large current densities of α-MoB_2 was benefited from its high conductivity (electrical resistivity of $(6.6 \pm 1.7) \times 10^{-7}$ Ω m) and large density of catalytic active sites. Furthermore, the catalytic activity trends of the four Mo-B phases (decreasing in the order of α-$MoB_2 \gg \beta$-$MoB_2 > MoB > Mo_2B$) demonstrated that the presence of the borophene substructure in α-MoB_2 played a crucial role in catalysis. The Fokwa group also verified the boron-dependency of Mo-B electrocatalysts for HER [84].

Inspired by the correlation between high activity and borophene substructure of α-MoB_2 catalyst, more transition metal diborides containing 2D boron layers have attracted the interest of researchers. The Zou group combined both theoretical and experimental study to investigate the electrocatalytic activity of a family of 12 transition metal diborides for HER. According to the theoretical results, their HER activity increased from group IV B to group VIII metal diborides, and the d-band center can be deemed as a good descriptor of activity for transition metal diborides (Fig. 5d). The experimental results further identified that RuB_2 is a competitive catalyst with Pt-like activity (Fig. 5e), especially in alkaline solution [47]. In addition, FeB_2 and VB_2 have also been studied as high-performance catalysts for HER by the Geyer group and the Fokwa group, respectively [85,86]. Furthermore, in order to gain insight into the influence of boron atoms on the surface hydrogen adsorption and HER catalytic activity of boron-bearing intermetallics, the Zou group studied the metal-boron electronic interaction of a family of 15 transition metal monoborides. Because of the similar electronegativity of metal and B atoms, charge transfers between metal and boron ($<$0.15|e|) in metal borides are found to be very small. They found that the strong hybridization of metal d orbital and boron sp orbitals can modify the d-band center of metal atoms, resulting in a weaker hydrogen adsorption on the metal-terminated intermetallic surfaces than on the corresponding pure metal [47].

Recently, intermetallic borides as NRR electrocatalysts have also attracted great interests from researchers. Mbenes, the boron-analogues of Mxenes with 2D layered structure, are believed to be able to achieve high activity and large reaction region simultaneously for NRR. Using DFT calculations, the Zhang's group predicted the NRR electrocatalytic activity of 16 stable 2D MBenes representatives from four key aspects. After rational evaluation, they identified that 7 MBenes (including CrB, MoB, WB, Mo_2B, V_3B_4, $CrMnB_2$ and $CrFeB_2$) have the intrinsic basal plane activity for NRR, while suppressing competitive HER. Especially the $CrMnB_2$ has reached a record level of theoretical activity, with a limit potential of -0.22 V. Meanwhile, these 7 MBenes have the superior capability to reduce O^*/OH^* into H_2O^* under reaction conditions to prevent the active site blocking problem caused by surface oxidation, which is so-called "self-activating process". They also estimated that the active sites density of these MBenes could reach the order of 10^{19} m^{-2}. In another work, Zhou *et al.* researched the reaction sites of NRR on MBenes. The theoretical results show that due to the co-existence of the occupied and unoccupied p(d) states of boron (metal) atoms, both the surface boron and metal atoms of MBenes can serve as the active sites, and the boron reaction center provides superior activity [87].

The Qiao group modeled molybdenum borides (Mo_2B, α-MoB, and MoB_2) to investigate the electrochemical activity of metal borides toward NRR. The N_2 adsorption strength was found to be determined by the orbital hybrids between boron p-orbital and N_2 π^*-orbital, and the population on p-π^*-orbital. The isolated boron sites on Mo_2B have less filled p_z-orbital, which promotes the activation of N_2 and weakens the triple bond of dinitrogen. They further screened out Fe_2B, and Co_2B with isolated boron sites and moderate p_z orbital filling as potential candidates for NRR electrocatalysts. Although the researches of intermetallic borides on NRR are mainly based on DFT calculations, some of them have been experimentally proven to be high-performance NRR electrocatalysts, such as MoAlB single crystals and ZrB_2 nanocubes. The as-synthesized MoAlB SCs was first reported to afford an NH_3 yield of 9.2 μg h^{-1} cm^{-2} mg$^{-1}_{cat.}$ and a Faraday efficiency of 30.1% at -0.05 V *vs.* RHE [55].

3.2. Transition metal boride derived catalysts

Intermetallic borides have also got ahead some considerable progress as OER electrocatalysts. The intermetallic borides with promising OER activity are mainly concentrated in iron-based (*e.g.*, Fe_2B, FeB_2) [88], cobalt-based (*e.g.*, Co_2B, Co_3B) [89,90], nickel-based (*e.g.*, Ni_3B, Ni_xB) borides [89], and some ternary metal borides (*e.g.*, $AlFe_2B_2$, FeNiB, $(Ni_xCo_{1-x})_2B$) [91–93]. With the development of operando and *in situ* techniques, these non-oxide intermetallic borides were found generally not remain stable and undergo surface reconstruction to form metal oxides/hydroxides as the new active species *in situ* in the catalytic oxidation condition

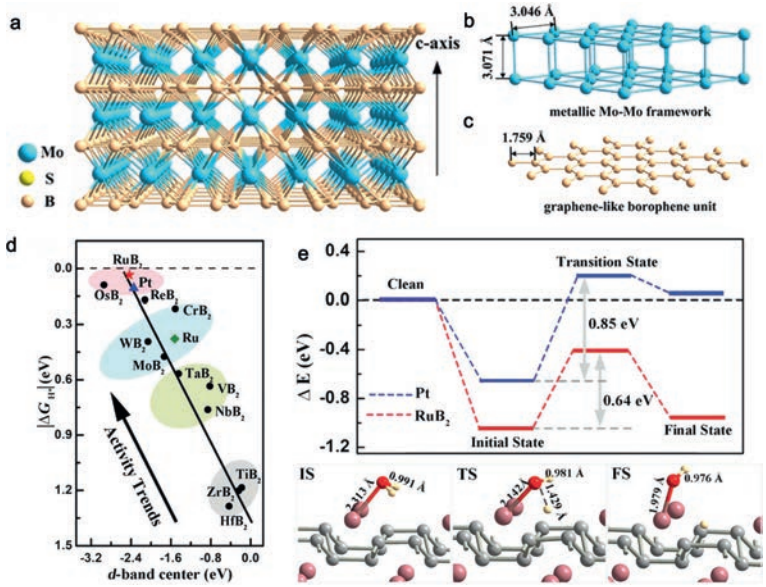

Fig. 5. (a) Crystal structure of α-MoB_2, in which Mo-Mo metallic bonds are not shown for clarity. (b) 3D metallic Mo-Mo framework in α-MoB_2. (c) 2D graphene-like borophene units in α-MoB_2. Reproduced with permission [37]. Copyright 2017, American Chemical Society. (d) Fitted linear relationship between hydrogen adsorption free energy (ΔG_{H^*}) and d-band center of MB_2, Pt, and Ru. (e) Reaction pathways for water molecule dissociation on the RuB_2 (001) and Pt (111) surfaces. Optimized structures for water molecule dissociation on the RuB_2 (001) surface in the initial state, transition state, and final state are shown in the side views. Ruthenium, boron, oxygen and hydrogen atoms are in pink, grey, red and yellow, respectively. Reproduced with permission [47]. Copyright 2019, Wiley-VCH.

of OER [94]. Noteblely, B atoms in the structure were depleted in the anodic polarization and were replaced by oxygen atoms, and the as-evolved products have been proven to be more active than the corresponding parent catalysts and the same catalyst materials synthesized directly [90]. Reasons for the activity improvement still call for investigations. Depending on materials structural features and experimental testing conditions (applied overpotential, electrolyte pH, temperature, pressure, *etc.*), the transformation can proceede completely or partially on the surface that core-shelled metal compounds coating with a layer of metal oxides/hydroxides were often obtained during the catalysis. A thorough understanding on the behavior of surface reconstruction process and the origin behind the scenario is of vital importance in proposing structure-composition-property relationships and unveiling the mechanism for OER as well as guiding our future research work.

As to metal borides, they are mainly encountered as pre-catalysts, that they can inevitably be oxidized into borates, boron oxides, and corresponding metal oxides/hydroxides *in situ*, making the latter the real catalytically active species. In 2017, Schuhmann *et al.* reported the synthesis of ultrathin amorphous nickel boride (Ni_xB) nanosheets. The as-synthesized nanosheets can act as efficient OER catalyst with remarkable activity and stability that it drives the OER at 20 mA/cm^2 under only 0.28 V overpotential in 1.0 mol/L KOH. However, structural reconstruction occured on the surface and Ni-B core with nickel hydroxide shell (Ni-B@$Ni(OH)_2$) structure was obtained. Under the assitance of X-ray absorption fine structure (XAFS), the authors observed a contraction of the Ni-O bonds in NiOOH accompanied with increase in disorder of the layer and pointed out Ni-B@NiOOH (core@shell) structure to be active phase [95]. Furthermore, Yujin Chen and coworkers developed a serize of crystal Co_xB catalysts (x = 1 to 3) material to catalyze OER and the materials had an activity sequence of Co_2B > Co_3B > CoB. Co_2B exhibits the best OER activity, with a current density of 10 mA/cm^2 at an overpotential of 287 mV in 1 mol/L KOH solution, comparable to the state-of-art commercial IrO_2. By characterizing the structural morphology and valence state of the post-OER materials, the authors confimed the reconstruction of catalysts and further analyzed the OER catalytic mechanism. They found Co_xB coated with a thin layer of polycrystalline CoOOH with enriched defects was formed and the outermost CoOOH layer act as the real active sites [96]. The both literatures all found that thermodynamically stable lower valence metals converted into corresponding high valence state and they hold the view that transition metals in higher valance state are the active phases and are responsible for the enhancement in catalytic activity regardless of the effect of boron [97,98].

These researchers observed the surface structral reconstruction and proposed the as-evolved oxyhydroxides are active sites in the reaction in regardless of B. Schuhmann *et al.* noticed this and detected B in the samples after catalysis in their experiment. They found B was still exist in the post-OER material and several existing forms were proposed. However, they failed to disclose the effect of B in catalysis [90]. With researches going on, the role of B has been gradually revealed. Some researchers claimed that B aslo made contribution to the surface reconstruction and played a positive role in activity enhancement. The Li group reported a core-shell structure consisting of a Ni^{II}-B_i shell on a nickel boride (NB) nanoparticle core, namely, Ni-B_i@NB to serve as efficient OER electrocatalyst (Figs. 6a–c) [99]. In addition, they found the crystallinity of the outermost Ni^{II}-B_i shell was tunable and in turn modulate material's OER activity. Crystallinity is neither the higher the better nor the lower the better that the partially crystallined Ni-B_i@NB (pc-Ni-B_i@NB) catalyst exhibits the best activity with an overpotential of only 302 mV, which is 23 mV less than that of the commercial IrO_2 catalyst. The surface composition was characterized to consist of only B_2O_3 and Ni-B_i, as B_2O_3 was inactive to the reaction, the activity was considered to be originated from Ni-B_i. The authors attributted the enhanced performance to the higher intrinsic OER catalytic activity of partially crystalline Ni-B_i with the more grain boundaries, point and line defects, undercoordinated sites, and edges at steps or kinks due to its partially crystalline nature. Just recently, Liang *et al.* recognized metal borides *in-situ* formed metal borates are responsible for their high activity and synthesized NiFe-Boride as a templating pre-catalyst to form an active NiFe-Borate catalyst. The derived metal oxides/borates

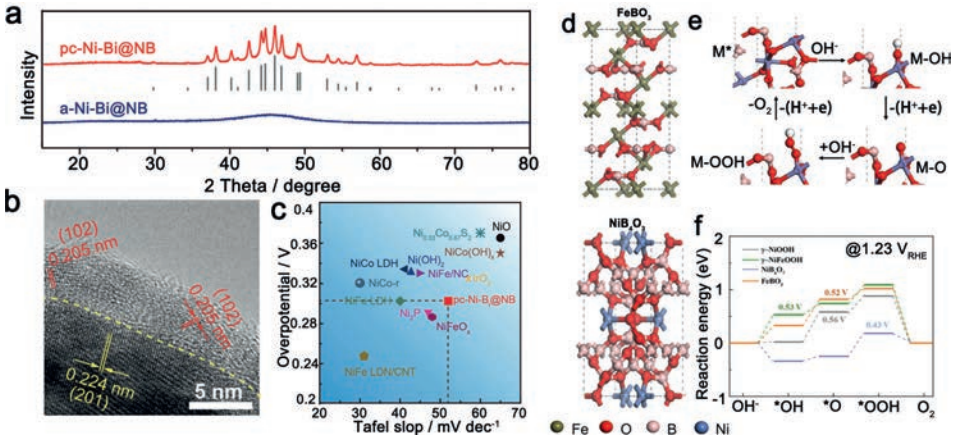

Fig. 6. (a) XRD patterns of a-Ni-B_i@NB and pc-Ni-B_i@NB. (b) HRTEM images of pc-Ni-B_i@NB. (c) Overpotential at 10 mA/cm^2 and Tafel slope of the state-of-the-art OER electrocatalysts supported on glass carbon electrodes in 1 mol/L KOH. Reproduced with permission [99]. Copyright 2017, Wiley-VCH. (d) The cell configurations of NiB_4O_7 and $FeBO_3$. (e) The schematic illustration of the 4-step OER pathway. (f) Predicted OER reaction energy diagram for NiB_4O_7, $FeBO_3$, γ-NiOOH, and γ-NiFeOOH in the alkaline electrolyte at 1.23 V *vs.* RHE. Reproduced with permission [39]. Copyright 2021, Nature Publishing Group.

can catalyze oxygen evolution efficiently with an overpotential of 167 mV at 10 mA/cm^2 and maintain its performance for over 400 h at current density of 1 A/cm^2, surpassing the benchmark of IrO_2 and RuO_2. Borate remained in the NiFe after catalysis as confirmed by *operando* spectroscopies. Comprehensive considering experimental findings and DFT calculations, they concluded that the *in-situ* formed new phase NiB_4O_7 and $FeBO_3$ can function as active site to facilitate $^*O \rightarrow {}^*OOH$ (Figs. 6d–f), enhancing the electrocatalytic activity of NiFe-Boride in OER [39].

Guo *et al.* prepared surface-activated amorphous Fe_xB catalysts, Fe–B–O@Fe_2B and Fe–B–O@FeB_2 by the reaction of alkali borohydride and corresponding iron salt followed by a simple oxidation treatment in air. They exhibited remarkable catalytic activity toward OER that they needed overpotential of 273 and 260 mV to deliver a current density of 10 mA/cm^2. They realized straightforward preparation of metal boride with active surface. Chemical surface state changes of products after OER was observed, reconstruction of surface structure and reproduction of the active surface was suggested. XPS results revealed the oxidation layer on the surface to be metal oxide/hydroxide and borate moieties, the newly formed species was considered to be the active phase and played a synergistic effect on the promotion of OER activity was proposed [88]. Gao *et al.* also revealed that in the active layer of Fe_2B NWs covered with metaborate and FeOOH, the metaborate species can improve the catalytic stability and activity [93].

The Zou group also devoted to the synthesis and electrochemical water splitting catalytic investigation of transition metal borides and proposed that the catalytically active phases are BO_2^-. In 2019, the Zou group adopted a boronization strategy to transform a series of metal sheets (including Ni, Co, Fe, NiFe alloys and steel sheets) into M_2B borides layers on the corresponding metal sheets, which can be used as highly active and stable, corrosion resistant oxygen evolution electrodes. The OER activities of boronized metal sheets are an order of magnitude higher than those of the corresponding metal sheets. In particular, the boronized NiFe alloy exhibits better intrinsic catalytic activity than the state-of-the-art materials, which overcome the overpotential barrier of 320 mV for OER. The boronized NiFe alloy can be stably operated in 1 mol/L KOH for more than 3000 h. Comparative XPS analysis of Ni and B in primary and post-OER material revealed surface of the boronized Ni sheet is further oxidized into γ-NiOOH films and boron species into metaborate. They demonstrated that the catalytic active phase for the boronized metal sheets is the *in situ* formed, amorphous, ultrathin (2–5 nm), metaborate-containing oxyhydroxide thin films [56].

Subsequently, the team designed a multilayered oxygen-evolution electrode, composing of the surface oxidized $NiFeB_x$ alloy layer as the catalytic active layer, the $NiFeB_x$ alloy interlayer as the corrosion-proof layer, and the NiFe alloy as structural support. *In situ* Raman techniques were used to unravel the interfacial electrocatalytic behavior of boronized nickel sheet during the electrochemical process. Authors observed phase transformation from $Ni(OH)_2$ to NiOOH under testing potential conditions and γ-NiOOH was preferentially formed in the presence of Fe dopants. They pointed out that the boron species are present in the form of metaborate in the outermost oxidized NiFeBx layer, and their existence is conductive to the generation and stabilization of the catalytic active phase γ-(Ni,Fe)OOH. Furthermore, DFT calculations demonstrated that metaborate modified γ-(Ni,Fe)OOH can achieve a relatively optimized adsorption with intermediates and hence higher intrinsic catalytic activity [100]. Though the evolution and working way of B in facilitating OER process is still controversial, the above findings together with the advanced *in-situ* characterization enlighten us to further explore the dynamic mechanism and manipulate the *in situ* catalyst surface reconstruction rationally.

3.3. Boron-doped catalysts

Heteroatom doping in catalysts is considered to be an effective strategy to adjust the electronic structures and/or electronic conductivity, thereby improving the electrocatalytic activity. Interestingly, the electronic structures of catalysts can be engineered to varied degrees according to the species and concentration of dopants. So far, a series of catalysts doped with metallic atoms (Fe, Co, Ni, *etc.*) and non-metallic atoms (N, P, S, *etc.*) have achieved great breakthroughs [101–105]. Different from the most widely investigated non-metallic dopant nitrogen, boron is less electronegative and is an important dopant that can exhibit novel properties. Therefore, boron-doped catalysts have attracted widespread attention in many electrocatalytic fields. Due to the small atomic radii, boron elements have been known to easily incorporate into the interstitial sites of metal lattices. The interstitial boron atoms can regulate the surface adsorption property and catalytic activity through multiple effects such as strain and ligand effects. This section focuses on the application of boron-doped catalysts in many reactions like CO_2RR, ORR and NRR.

CO_2RR on Pd is an electrocatalytic system model for fundamental research. In 2018, the Jiang group explored a boron-doped Pd catalyst (Pd-B/C) for electrocatalytic CO_2 RR over the potential range of −0.2 V to −1.0 V (*vs.* RHE) [106]. They found that the B-doping in the Pd lattice interstice made the adsorption energy of HCOO* more negative than that of *COOH, thereby improving the CO tolerance of Pd-B and facilitating the selectivity of the formic acid pathway. Specifically, the Pd-B/C obtained a Faradaic efficiency of ∼70% for formate after 2 h of electrolysis at −0.5 V, leading to a formate concentration of 234 mmol L^{-1} $mg_{Pd}{}^{-1}$, which was about 18 times as high as that on Pd/C. In 2021, the Cai group further conducted an *in situ* spectroscopic study on the electrocatalytic CO_2 RR on Pd and Pd-B electrodes. This work provided a direct observation at molecular level of the role of surface CO as well as the B-doping effect at varied potentials. The results revealed that at lower overpotentials, CO gradually accumulated to poison the dominant formate pathway, while at higher overpotentials, the linearly bonded CO (CO_L) species acted as an active precursors for CO gas production, and the strongly adsorbed bridge-bonded CO (CO_B) act as the spectators or poisoning species. They also confirmed the inhibiting effect of boron-doping in Pd electrode on CO production and the promoting effect on formate formation [107].

In another study on Cu-based electrocatalysts for CO_2 RR, Sargent *et al.* used boron to tune the ratio of $Cu^{\delta+}$ to Cu^0 active sites, thereby improving both stability and C_2-product generation. By the *in situ* X-ray absorption near-edge spectroscopy (XANES), the average oxidation state of copper in the Cu(B) samples was found to vary from 0 to +1 with the increase of B content. The Cu(B)-2 with an average copper valence of +0.35 exhibited an impressive C_2 Faradaic efficiency of about 80%, and maintained a high C_2 selectivity over a wide potential window of −0.9∼−1.2 V *vs.* RHE. The high selectivity of C_2 products is attributed to the regulation of the average copper oxidation state by the boron dopant, which enable the control over CO adsorption and dimerization [108]. Recently, the Schuhmann group has developed B-doped Cu (B-Cu) and B-Cu-Zn gas diffusion electrodes to efficiently and stably convert CO_2 into C_{2+} products efficiently and stably at industrially relevant current densities. The B-Cu catalyst was tested to have high activity and selectivity, and its long-term stability for C_{2+} formation can be improved by incorporating an optimal amount of Zn [109].

In electrocatalytic ORR, it was found that B-doping can also weaken the surface adsorption energy of oxygen-containing intermediates to promote ORR catalytic activity. The B-doped Pd material (Pd-B) synthesized by Sato's group exhibits 2.2 times and 8.8 times higher specific activity and 14 times and 35 times less costly than commercial pure Pd and Pt catalysts, respectively. Combining DFT calculations and X-ray photoelectron spectroscopy (XPS), they found that the B-doping negatively shifted the surface core level of Pd, which implies that electrons are transferred from Pd to B atoms, and the additional electrons on Pd-B surface would weaken O bonding to Pd and improve catalytic activity [57]. For Pd-B catalysts, Chen *et al.* explored three types of surface sites, including Pd-BO_2 assemblies, neighboring Pd-BO_2 assemblies, Pd atoms, and subsurface B modified Pd atoms, which were responsible for enhancing ORR activity (Fig. 7). The oxophilicity of both neighboring Pd-BO_2 assemblies Pd atoms and subsurface B modified Pd atoms were found to near the top of the activity volcano plot for ORR. This means that these two types of Pd atoms sites could catalyze ORR much more efficiently than Pt. Meanwhile, the O adsorption energy at Pd-BO_2 assemblies sites is ∼0.4 eV more positive than that of Pt, which suggests that these sites have Pt-like activity. The mass and specific activity of the synthesized B-Pd nanoalloy on ORR are about 14 and 14.6 times higher than that of state-of-the-art commercial Pt catalyst, respectively [110].

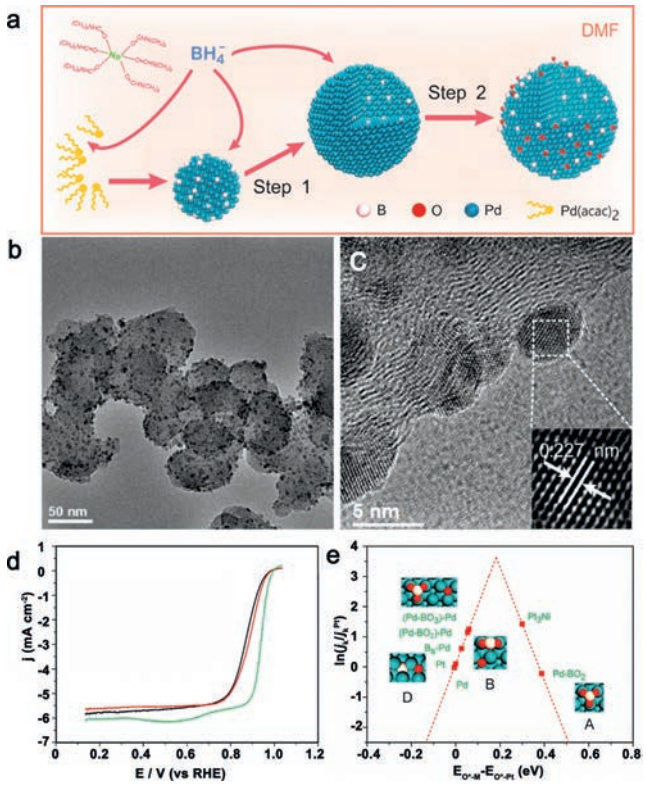

Fig. 7. (a) Illustrations of the synthesis procedure and formation mechanism of B-Pd/C. (b) Representative TEM image and (c) HRTEM image of B-Pd/C. (d) ORR polarization curves for B-Pd/C, Pd/C and Pt/C; the inset in (d) is the mass and specific activity at 0.9 V. (e) ORR activity of different surface sites on the B-Pd alloy surface, *versus* that on platinum. Reproduced with permission [110]. Copyright 2017, American Chemical Society.

In 2019, after exploring 21 boron-based concept NRR catalysts, the Sun group predicted that the single boron atom doped into h-MoS_2 or supported on graphene are promising catalysts with excellent activity and selectivity against HER. Subsequently, the Tang group compared the difference between diatomic boron doped single-layer MoS_2 (B_2@MoS_2) and single boron atom doped single-layer MoS_2 (B@MoS_2) as NRR catalysts in terms of thermodynamics, selectivity, and kinetics analysis. It was found that B_2@MoS_2 showed excellent structural and thermodynamic stability, and significant improvement in the conductivity as compared to that of MoS_2. Due to the efficient electron transfer and the synergistic effect of diatomic boron, B_2@MoS_2 exhibited better N_2 capture and reduction activity [111]. Chu *et al.* found that boron-doping in MnO_2 nanosheets can induce abundant oxygen-vacancies, which can synergistically promote the conductivity and enhance the intrinsic NRR activity. By DFT calculations, they further revealed that the synergistic effect of boron-doping and oxygen-vacancies cause the asymmetric charge distribution, which activates neighboring Mn atoms for stabilizing the key intermediate $*N_2H$ on MnO_2 and lowering the reaction energy barrier [112].

In addition to boron-doped metal-based catalysts, some boron-doped non-metal materials for electrocatalysis have also been developed, mainly boron-doped carbon materials. Compared with metal-based catalysts, these metal-free catalysts have obvious advantages, such as low cost, high stability. Zheng *et al.* developed a boron-doped graphene NRR electrocatalyst, in which boron-doping leads to redistribution of electron density, and the electron-deficient boron sites enhance the binding capability with N_2 molecules. DFT calculation results revealed that among several types of boron-doped carbon structures, the G-like BC_3-type struc-

ture had the lowest energy barrier for electro-reducing nitrogen to ammonia. The NH_3 production rate and Faraday efficiency of boron-doped graphene with a doping level of 6.2% are 9.8 μg h^{-1} cm^{-2} and 10.8% at −0.5 V *vs.* RHE, respectively [113]. Yasuaki *et al.* studied a boron-doped diamond (BDD) electrode used in a two-compartment flow cell, which can efficiently electrochemically reduce CO_2 to formic acid, with a Faraday efficiency of 94.7% and a selectivity of over 99% [114]. Earlier, the Ma group developed a boron-doped carbon nanotubes electrocatalyst, which exhibited a good ORR performance in electrocatalytic activity, stability and immunity to methanol crossover and CO poisoning [115].

3.4. Metal boride-decorated catalysts

In addition to act as catalytic active phases, transition metal borides have recently been employed as cocatalysts in heterogeneous catalysis, especially in photocatalysis and photoelectrocatalysis. Precious metals Pt [116], Ru [117], Rh [118], Pd [119], Au [120] and Ag [121] have long been employed as traditional cocatalysts, which can improve the charge-separation efficiency by acting as electron sink to suppress electron-hole pairs recombination and provide abundant active sites for the proton-reduction reaction at the same time. Yet the high price and scarcity hampere the pratical application of noble-metal based cocatalysts in energy production. Therefore, developing new cocatalysts constructing from inexpensive and earth-abundant elements can solve the bottleneck problem of photocatalytic development and hence have attracted tremdous research efforts. Suitable energy band structure, remarkable stability and easy availability are requisites to a good cocatalyst. Nanosized transition metal are a typical representative candidates family for their low cost, excellent chemical stability, nontoxicity, and high reactivity. It was since the Xu group reported the construction of Ni_xB/CdS composite to act as highly efficient photocatalyst with H_2 production rate of 4.8 mmol h^{-1} g^{-1} in 2015, transition metal borides have attracted trmendous research interest in photocatalysis. Ni_xB/CdS composite was synthesized by a simple reduction reaction and found to be 20 times more efficient than that of CdS alone. Related characterization and assumption were presented in therir report, however, the mechanism on the performance enhancement was ambigious [122]. Subsequently, the Bao group optimized the photocatalytic activity of Ta_2O_5 by surface decorating Ta_3B_2. Experimental results showed that Ta_3B_2 combined tightly with Ta_2O_5 to form a core-shell Ta_2O_5/Ta_3B_2 heterostructure. Hybrid structure offered good interfacial contact and therotical calculation revealed that boron doping in Ta_2O_5-OVs can modify the surface electronic structure of Ta_2O_5 from semiconductor to metallic states [123]. The Zhang group reported amorphous nickel boride (NiB) dispersed uniformly over graphite carbon nitride (C_3N_4) with higher hydrogen evolution performance. Proper loading amount of NiB on C_3N_4 leaded to remarkable HER activity of 464.4 μmol g^{-1} h^{-1} and apparent quantum yield of 10.92% with 365 nm light irradiation (Figs. 8a and b). The suitable band structure of NiB was consisdered to be responsible for the facilition that photoinduced electrons of C_3N_4 can quickly transfer to NiB nanoparticles through the B($\delta-$)–Ni($\delta+$)–N($\delta-$) bonds, followed by transfering to the active sites on the surface to participate in HER [124]. The above examples all indicated that deep colors and narrow band gaps of borides increased the light absorption and lowered activation energy for the H_2 evolution reaction. Furthermore, suitable band structure of the boride cocatalysts makes it accept electrons easily, which accelerates the electron-hole pair seperation and hence promotes reaction kinetics and maximizes utilization efficiency of solar energy.

Several factors, such as composition, crystal phase and loading amount, have been found to be critical in regulating the catalytic properties of metal borides-decorated photo(electro)catalysts. Li

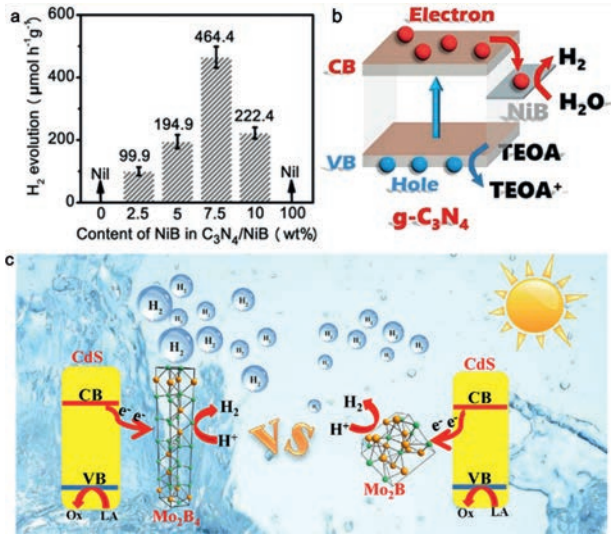

Fig. 8. (a) Photocatalytic hydrogen production rates on C_3N_4/NiB photocatalysts loaded with different amounts of NiB under the irradiation of a 300 W Xe lamp (AM1.5 air mass filter). (b) Charge separation and transfer in the C_3N_4/$NiB_{7.5}$ system under irradiation. Reproduced with permission [124]. Copyright 2018, American Chemical Society. (c) Proposed photocatalytic HER mechanisms of CdS-Mo_2B_4 (15 wt%, left) and CdS-Mo_2B (15 wt%, right). Boron and molybdenum are in green and orange, respectively. Reproduced with permission [127]. Copyright 2021, Elsevier Ltd.

et al. reported low-cost Ni_3B/$Ni(OH)_2$ can boost the photocatalytic H_2 production over g-C_3N_4 nanosheets. The Ni_3B/$Ni(OH)_2$ hybird was fabricated by reducing Ni^{2+} followed by photodeposition of $Ni(OH)_2$. Authors found the introduction of both Ni_3B and $Ni(OH)_2$ could narrow the band gap and promote the interficial charge trapping and separation efficiency. The main reason for the improved hydrogen generation was consisdered to be the facililated electron transfer from g-C_3N_4 to Ni_3B and then to $Ni(OH)_2$ through the intimate interface [125]. Loading amount is also of vital importance to the behavior of cocatalyst. For example, Zhao *et al.* found $MAPbI_3$ coupled with amorphous NiCoB with the amount of 30% possessed the maximum H_2 generation yield of 2625.57 μmol g^{-1} h^{-1}, exceeding that of Pt/$MAPbI_3$ and was 114 folds higher than its unloaded counterpart. The HER rate increased with the increasing of NiCoB amount and reached the top at the NiCoB content of 30%, while further increasing NiCoB amount cannot enhance hydrogen production any longer probebly because excessive NiCoB could affect the light absorption of $MAPbI_3$ and may block some active sites [126]. Due to the electron deficient features of B, local electron density of the interface of composits can be severly tuned and catalytic performance would be optimized. And recently, the Ding group investigated the influence of B content in MoB_x on photocatalytic HER activity. Coupling Mo_2B_x on CdS nanoparticles can significantly improve its photocatalytic HER performance (Fig. 8c). Mo_2B_4 decorated material performed obviously better in electron transfer and photocatalysis than that of Mo_2B, exhibiting MoB_x demonstrate a strong B dependence in photocatalytic HER. Owing to the electron deficient property of B, it attracts electron from neighboring CdS, then potential difference exists in the CdS/Mo_2B_4 hybird. Photoluminescence (PL) spectra and surface photovoltage spectroscopy (SPV) demonstrate that the photogenerated carrier signal for CdS/Mo_2B_x is stronger and lifetime is longer, indicating that the photogenerated charge is not easy to recombination. Inhibition of recombination may be because of the existence of Mo_2B_x, which can accept photogenerated electrons from the conduction band of CdS due to the presence of potential difference. So the

larger potential difference between CdS and B-rich Mo_2B_4 is benificial to electron transfer and hydrogen evolution process [127].

Apart from water splitting, transition metal borides are receiving increasing interest in various fields including photocatalytic CO_2 reduction reaction (CO_2RR). A recent study by Ye and coworkers demenstrated cocatalytic effect of the TMBs (Ni_3B, Co_3B and Fe_2B) for photocatalytic CO_2 reduction. The reaction converts CO_2 to valuable chemical fuels (such as CO, CH_4 and HCOOH) with solar energy, which not only address energy shortage but also alleviate the greenhouse effect. The authors found Ni_3B, Co_3B and Fe_2B were effective and low-cost cocatalysts in enhancing the performance of photocatalytic CO_2 reduction in the presence of $[Ru(bpy)_3]Cl_2$ as a light absorber under visible light, while TaB_2, NbB_2 and MoB were not. Ni_3B exhibits the highest activity among them of 157.7 mmol/h CO evolution rate and selectivity of 93.0%. Valence band XPS (VB-XPS) spectrum indicates that charges are accumulated on the Ni-B bond, making it electronic reservoir to transport electrons for metal active sites. Photoluminescence (PL) decay spectroscopy gave hint for dynamic charge behavior and revealed Ni_3B/[Ru] had the longest lifetime. Together with the DFT calculations, Ni-B bond in Ni_3B is beneficial for the desorption of the CO molecule in photocatalytic CO_2 process, the authors concluded that the highest catalytic performance of Ni_3B originated from its metallic character and the electron enriched Ni-B bond to provide abundant long-lived electrons and lower the overpotential for facilitating the CO_2 reduction [127]. This work provided a completely new application for borides, refreshed our understanding on it and enlightened us to explore more boride modified catalysts and act as promising cocatalyst candidates for more photocatalytic reactions (*i.e.* organic degradation, ethanol oxidition reaction and methane conversion).

3.5. Boron-containing compounds as catalyst supports

By dispersing metal catalysts on the appropriate supports, the catalysts can obtain high specific surface area and good dispersity, thereby fully exposing the catalytic active sites and improving the catalytic efficiency of active components per unit mass. Similar to graphene, the h-BN with layered structure has been widely used in various catalytic fields due to its low density, large surface area, unique electronic properties, excellent thermal and chemical stability [128]. However, the progress of h-BN as an electrocatalyst support is relatively slow, mainly for the following two reasons: (1) h-BN has low electrical conductivity because of the interlaminar insulation and wide band gap; (2) h-BN has better resistance of oxidation and intercalation than graphene, so it is difficult to exfoliate h-BN through conventional routes [129]. In recent years, many theoretical and experimental results have indicated that the conductivity and band gap of h-BN can be tuned through chemical modifications, *e.g.*, vacancy defects, hetero-atom dopants or metal substrates (Fig. 9) [130]. At the same time, a variety of improved methods have been developed to synthesize stable 2D h-BN nanostructures which can be used to support and disperse metal atoms. These studies have renewed researchers' interests in h-BN as an electrocatalyst support for energy conversion.

Although Pt-based nanomaterials are the state-of-the-art catalyst for the ORR at cathode of proton exchange membrane fuel cells, they still face the problem of activity deterioration. In order to improve the durability and activity of Pt-based electrocatalyst for ORR, the Li group employed porous boron nitride (p-BN) as functional support to stabilize ultrafine Pt nanoparticles (Pt/p-BN) and engineer its electronic structure. The experimental results show that the Pt/p-BN exhibits significantly enhanced ORR activity with ~53 mV positive shift of half-wave potential compared to commercial Pt/C. After 10,000-potential cycle durability tests, the electrochemical active surface area of Pt/p-BN remains almost unaltered, and the ORR half-wave potential only negatively shifts by 2 mV. They further studied the synergistic co-catalytic effect between Pt NPs and p-BN by DFT calculations. It was found that electrons transfer from electron-rich N atoms to Pt NPs, and from Pt NPs to electron-deficient B atoms, resulting in an electron donation-back donation process [131]. This process strengthens the bonding between Pt NPs and p-BN, and optimizes the electronic structure of Pt. Besides Pt nanoparticles, Li's group studied the isolated Au atom supported on defective p-BN ($Au/p\text{-}BN\text{-}V_N$) in term of stability, catalytic activity and catalytic mechanisms. The defective p-BN also has a strong anchoring effect on Au atoms. They predicted that $Au/p\text{-}BN\text{-}V_N$ was an effective ORR catalyst according to frontier molecular orbital and charge-density analysis [132].

Combining experiments and DFT calculations, the Sun group designed and synthesized h-BN/Pd as a durable and efficient hetero-structured electrocatalyst for ORR. The h-BN has been demonstrated as a robust catalyst support, whilch not only suppresses the agglomeration of Pd NPs, maximizes the exposure of active sites, but also endows the heterostructures with a superhydrophobic surface, facilitating the adsorption capability and diffusion kinetics of O_2. The strong interaction between h-BN and Pd can downshift the Pd d-band center, thereby optimizing the affinity with the oxygen-containing reaction intermediate [130]. Another nanocomposite catalyst composed of MnO_2 nanorods supported on h-BN and carbon has been reported [132]. The catalyst exhibits a substantially higher onset potential of 0.9 V *vs.* RHE and limiting kinetic current density of 5.6 mA/cm^2 at 1600 rpm for the ORR. Furthermore, it is theoretically confirmed that single Co atoms, Pd_xCu_{4-x} subnanoclusters supported on defective 2D BN can be used as ORR electrocatalysts [133].

Since TMN_x (TM = transition metal) compounds exhibit high catalytic activity for NRR, the unsaturated N atoms around B monovacancy in a defective BN nanosheet have been studied to immobilize single metal atoms for nitrogen activation. By means of DFT computations, the Zhao group screened the NRR potentials of a series of single TM atoms (TM = Sc to Zn, Mo, Ru, Rh, Pd and Ag) supported on the defective BN monolayer with B monovacancy. They found that the single Mo atom supported on BN nanosheet possesses the highest NRR catalytic activity at room temperature through an enzymatic mechanism with a quite low overpotential of 0.19 V. And high spin-polarization, selective stabilization of N_2H^* or destabilizing $NH_2{}^*$ species are the main reasons for the high activity of Mo-embedded BN nanosheet [134]. The Jiang group creatively introduced graphene to design a single TM atom sandwiched between h-BN and graphene sheets (namely, BN/TM/G, TM = Sc, Ti, V, Cr, Mn, Fe, Co, Ni, Cu, Zr, Nb, Mo, Ru, Rh and Pd) as an efficient single-atom catalyst (SAC) for the electrochemical NRR. They found that these sandwich structures can form stable and tunable polarization interface polarization fields, which enable the TM atoms to donate electrons to neighboring B atoms. The B atoms serve as active sites for N_2 capture and activation through the electronic acceptance-donation process. BN/V/G and BN/Ti/G systems were evaluated as promising NRR electrocatalysts with high activity and selectivity [135].

In experiments, Shanmugam *et al.* demonstrated a single step *in-situ* nitridation method to support cubic molybdenum nitride (γ-Mo_2N) nanoparticles on a 2D h-BN sheet as a cost-effective NRR electrocatalyst. EPR and Raman investigations suggested that the nanoparticle size governs the provocation of N-vacancies, and the fine-tuning of their significance emanates the highest Faradaic efficiency of 61.5% and NH_3 yield rate of 58.5 μg h^{-1} mg^{-1} [136]. In addition to the NRR and ORR, h-BN-supported electrocatalysts have also been developed for other electrocatalytic reactions. For example, Back and Siahrostami have used BN nanosheets to anchor bimetallic Pd-Fe nanoparticles for Suzuki-Miyaura coupling cata-

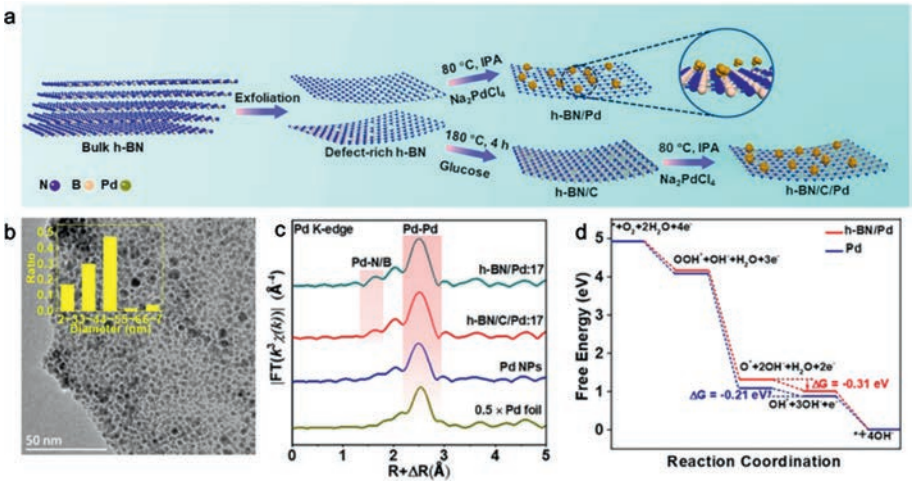

Fig. 9. (a) Schematic illustration showing exfoliation of h-BN and preparation of h-BN/Pd and h-BN/C/Pd. (b) TEM of h-BN/C/Pd:17 (inset: particle size distribution of Pd NPs). (c) Pd Kedge k^3-weighted EXAFS oscillations. (d) Free energy diagrams during the ORR at $U = 0$ V *vs.* NHE. Reproduced with permission [130]. Copyright 2020, American Chemical Society.

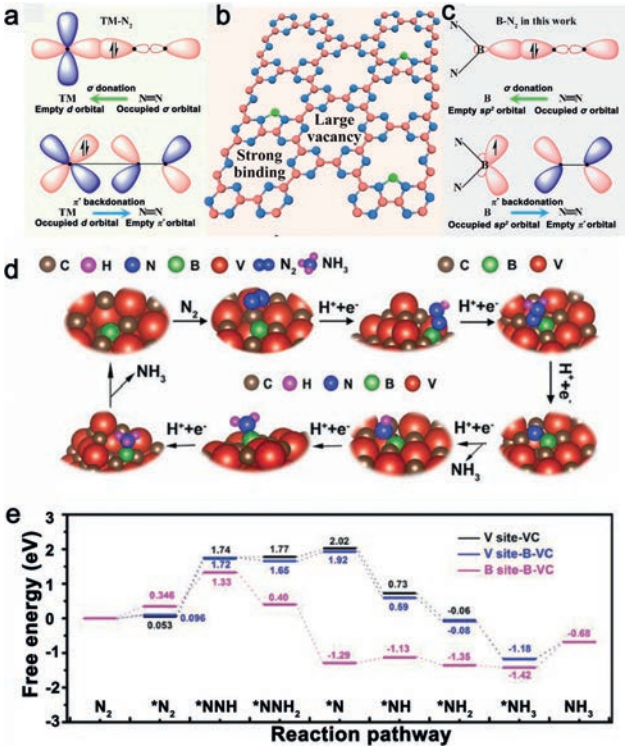

Fig. 10. (a) Simplified schematic of N_2 bonding to transition metals. (b) Design concept of B atom decoration on g-CN. The B atom bonds with two N atoms of g-CN to form two B−N bonds, leaving one half-occupied sp^2 orbital and one empty sp^2 orbital. Therefore, the as-designed B@gCN can facilitate the binding and activation of N_2. (c) Schematic of N_2 bonding to B atom on B@g-CN. Reproduced with permission [140]. Copyright 2019, American Chemical Society. (d) DFT-calculated eNRR reaction cycle through distal pathway on the B site in B-VC model. (e) Free energy diagrams of distal eNRR pathway on the V site of VC, V site of B-VC and B site of B-VC. Reproduced with permission [139]. Copyright 2021, Wiley-VCH.

lysts [128]; Liu *et al.* used the laser-modified BN with C, O dopants to load IrO_x for the oxygen evolution [137].

Strong metal-support interactions (SMSI) are essencial to supported nanoparticle catalysts for multiple functions include increasing supported metal dispersion, promoting charge transfer, and so on. Besides BN catalyst support, metal boride has recently emerged to act as promising support because of high electrical conductivity, high melting point and the ability to offer SMSI like that in classical metal/oxide catalyst structure. Noble metals play an important role in heterogeneous catalysis. Reducing usage is the main challenge for their low abundance. In this sense, combining the advantages of metal boride and noble metal to construct SMSI may have great potential to achieve highly active and stable catalyst for efficient hydrogenation. Li *et al.* confirmed the SMSI between noble metal Pt and 2D TiB_2 supports [75]. The TiO_x-terminated TiB_2 surfaces are the active sites catalyzing the dehydrogenation of formic acid at room temperature. The Pt/TiB_2 catalyst displayed an outstanding hydrogen productivity of 13.8 mmol $g^{-1}{}_{cat}$ h^{-1} and >99.9% selectivity toward CO_2 and H_2. Interplay between covalent and electrostatic interactions is resonable for the stabilization of TiB_2 overlayers, as suggestted by computational results. Such progresses undoubtedly make a step forward in supported nanoparticle catalyst development. However, some critical matters still need to be carefully considered in catalyst design, for example, construction of layered structure and/or porous structure of metal boride, anti oxidation of boride substrate, *etc.* Therefore, new discoveries and comprehending of new boride supporting nanoparticles with strong SMSI are important in the design and application of supported catalysts.

3.6. Single-boron-site catalysts

Single atom catalysts generally refer to isolated metal centers which coordinate with either nonmetal atoms (such as N, O atoms) or other metal atoms, usually acting as highly active catalytic sites towards a specific reaction. With the vigorous development of energy-related catalytic applications, non-metallic single atoms (especially single site boron) have attracted more attention in recent years. In these single-boron-site catalysts, boron atoms are spatially separated by metal atoms or other non-metallic atoms, and they do not directly bond to a second boron atom. Some single-boron-site catalysts were found highly efficient to some catalytic process especially in NRR. This is due to good interaction between electronic structure of single boron matches that of nitrogen molecule [16]. The unique combination of unoccupied p orbitals as well as lone-pair electrons at the same boron atom, which can accept σ donation from triple bond of nitrogen and give π backdonation to N_2, enhances the N_2 adsorption and activation, facilitating intermediate transferring.

The understanding of single-boron-site starts with the research of Legare and co-workers in 2018 [16]. They reported N_2 bind-

ing and reduction by a dicoordinate borylene that central N_2 unit could bind to two borylene fragments through their boron atoms and resulted in either neutral (B_2N_2) or dianionic ($[B_2N_2]^{2-}$) as products. The experiment was achieved at −80 °C with the existance of KC_8, which is critical and harch. With their continuous efforts, they realized room-temperature conversion of dinitrogen to ammonium by a one-pot binding strategy. They discovered the direct binding of dinitrogen to boron in the complex [((CAAC)(Dur)B)$_2$(N_2)] in an end-on bridging fashion and multiple reduction-protonation steps cleavage of the N-N triple bond and total reduction of N_2 to 2 equiv. of ammonia on B sites [138]. The above two examples and related research enlightened scientists to study single B sites supported in C and N containing materials and their application towards conversion nitrogen to ammonia in recent years. Inspired by the biological process one could envisage N_2 fixation to occur on the surface of inorganic solid materials, which are efficient and recyclable. These findings and related study make researchers relized B sites coordinated by nitrogen and carbon atoms are ideal research model for experimental and calculations.

To investigate the single B sites in CN materials, some theoretical models were built for catalytic studies (Fig. 10) [139,140]. Dai *et al.* theoretically reported single B atom supported on holey g-CN (B@*g*-CN) can serve as metal-free photocatalyst for highly efficient N_2 fixation and reduction on the basis of the "σ donation−π^* back-donation". The centralized spin-polarization on the B atom, reduced exciton binding energy and efficient prohibition of competitive HER were considered as key factors of high reactivity and selectivity for NRR. In addition, they theoretically disclosed that the external potential provided by photogenerated electrons for NRR/HER endowing B@*g*-CN spontaneous catalyze NRR and inaccessible HER [140]. Lately, the Wang group performed extensive first-principles calculations on B sites with different electronic configurations (*i.e.*, sp^{2-} and sp^{3-} hybridized B species) in C_2N [141]. They found both sp^{2-} and sp^{3-} hybridized B can fix and reduce dinitrogen efficiently only sp^3-B fails to suppress the competing hydrogen evolution. They clearly plot the activity and selectivity of sp^{2-} and sp^{3-} B for NRR and more importantly build up the structure-performance correlations. Mechanism on how B site participates in the process of nitrogen fixation was also disclosed that the π^* orbital of N_2 interacts with the two sp^3 orbitals of B with similar symmetry and appropriate energy *via* a p-bonding interaction, leading to lone pair electrons of nitrogen transfer to the empty orbit of B and electron back-donation from the filled B sp^3 orbital into the empty p^* state of N_2. The nitrogen triple bond is thus substantially weakened and N_2 adsorption is simultaneously stabilized.

Apart from nonmetallic atoms isolated single B sites, researchers have also devoted to construct appropriate structure to achieve single B sites isolated by metallic atoms and delve into their catalytic behavior. For example, Chen *et al.* rationally designed and synthesized isolated single-B atoms in intermetallic carbide as NRR catalyst with enhanced selectivity [139]. The contiguous boron atoms in the ordered intermetallic structure of vanadium carbide (VC) was isolated into single B-sites with specific electronic structures. The electron deficient boron sites triggered charge density redistribution in the hybird material, exhibiting excellent selectivity towards NRR. DFT calculations revealed that the unique configuration could regulate local electron density of the composite through B-C-V bond and effectively favor the N_2 adsorption, activation, and hydrogenation process, endowing the distinguished activity and selectivity, as evidenced by excellent Faradaic efficiency of 46.1% and NH_3 yield of 0.443 μmol h^{-1} cm^{-2}.

Boron doping into the graphene framework leads to the redistribution of electron density, making the electron deficient boron position provides enhanced binding ability with N_2 molecules. DFT calculations reveal the catalytic activities of different boron doped carbon structures and suggest BC_3 structure give the lowest energy barrier of N_2 electroreduction to NH_3 [113]. The boron-doped graphene with a doping level of 6.2% achieved a NH_3 production rate of 9.8 mg h^{-1} cm^{-2} and an excellent Faradic efficiency (10.8% at −0.5 V *vs.* RHE). In addition to its application in NRR reaction, single boron site catalysts are also expected to be applied in other energy conversion reactions.

4. Conclusions and outlook

Boron-containing materials have been emerging as an important branch of heterogeneous catalysts for their unexpected catalytic performance presented. Identification the roles of boron in the material systems and design of the composition and structure of boron-containing materials are important for catalysis research. We have reviewed the applications of boron-containing materials in heterogeneous catalysis in detail. We discussed the existing forms of boron in these compounds, and highlighted their roles in heterogeneous catalysis and interpret how they work. Although significant progress has been made, there are still some challenges to be further addressed in future research.

(1) Rational design and accurate synthesis of boron-containing catalysts. Traditional preparation of ordered metal borides in pure phase often requires harsh conditions, high pressure and/or high temperature. Developing mild, green and energy saving methods for massive preparations of intermetallic boride is necessary. The obtained boride products are generally large in size due to the high temperature/high pressure conditions, which limit the morphology and size control of borides and hamper their applications in catalysis or as catalyst supports. From this point of view, developing synthetic methods to prepare nano borides with specific morphology, crystal phase and exposed crystal facet is vital to boride family. To boron-doped catalyst system, controlling the position, concentration and order of boron atoms in the host is still a great challenge and an important research direction in the future.

(2) Establishment of clear structure-activity relationship in boron-containing catalysts. For boride catalysts, introducing boron into metal lattice brings a series of geometric and electronic structure regulation effects, such as lattice expansion, crystal phase transition, charge transfer, orbital hybridization and so forth. It is really hard work to accurately identify the contribution of each effect on the catalytic reaction. Theoretical calculation and accurate design of comparative experiment may bring a turn for the better. For boron doping systems, observing the existing position and form of B experimentally is still a great challenge due to the small size, uneven distribution and low content of boron in the metal lattice. Using advanced characterization methods, such as aberration-corrected scanning TEM (STEM), X-ray pair distribution function (XPDF) and synchrotron X-ray absorption spectroscopy (XAS), are of significant importance to study the existing forms and chemical properties of boron in catalysts, as well as to reveal the roles of boron play in catalysis. The surface or the whole bulk of some boride catalysts would undergo self-reconstruction during electrocatalysis, because of metal ions leaching out or being oxidized under electrocatalytic conditions. Thus, it is very important to reveal their evolution pattern by means of *in-situ* microscopy, diffraction and spectroscopy.

(3) Exploiting new boron-containing catalysts toward various chemical reactions. The present research on boride catalysts

is mainly focused on binary, and ternary and even multicomponent borides receive rare attention, which deserve further theoretical and experimental study. For boron doping system, current research focuses on boron doping in metal lattice, while boron doping in carbon-based catalytic materials is less when compared with the doping of other non-metallic atoms such as N, S and P. Furthermore, multi-doping, such as nitrogen and boron co-doping, is also an effective strategy for optimizing materials' catalytic properties.

In view of the above challenges, we propose the following directions for future development of boron-containing catalysts [142]. Theoretical calculation and simulation will be popular in accurate prediction and screening of boron containing catalysts for its instructive and effective effect. More accurate *in situ* characterization to study the existing valence of boron and evolution process of boron-containing catalysts will be developed to learn about reaction mechanism and in turn guide catalysts design. More green and mild preparation of boron-based catalysts is appealing to environmental protection and sustainable development, and attracts more research interest. Boron containing catalysts can make a significant contribution to a much broader range of catalytic reactions. For example, metal borides could be considered as efficient electrocatalysts for some new electrosynthesis and photosynthetic reactions such as H_2O_2 generation.

Declaration of competing interest

The authors declare that they have no known competing financial interests or personal relationships that could have appeared to influence the work reported in this paper.

Acknowledgments

X. Zou thanks for the financial support from the National Natural Science Foundation of China (NSFC Nos. 21922507 and 21771079), the Jilin Province Science and Technology Development Plan (No. YDZJ202101ZYTS126), and the Fundamental Research Funds for the Central Universities. X. He thanks for the financial support from Natural Science Foundation of Jilin Province, China (No. 20210101120JC).

References

[1] M.V. Pahl, B.D. Culver, N.D. Vaziri, J. Renal Nutr. 15 (2005) 362–370.
[2] A. Huang, X. Chen, C. Wang, Z. Wang, Mater. Res. Express 6 (2018) 025036.
[3] H.J. Zhai, B. Kiran, J. Li, L.S. Wang, Nat. Mater. 2 (2003) 827–833.
[4] B. Albert, H. Hillebrecht, Angew. Chem. Int. Ed. 48 (2009) 8640–8668.
[5] A.R. Oganov, J. Chen, C. Gatti, et al., Nature 457 (2009) 863–867.
[6] A. Banks, J. Chem. Educ. 67 (1990) 14.
[7] C.G. Woodbridge, Sci. Mon. 70 (1950) 97–104.
[8] J.A. Moore, Expert Scientific Committee, Reprod. Toxicol. 11 (1997) 123–160.
[9] D.M. Schubert, Struct. Bond. 105 (2003) 1–40.
[10] C.A. Rosolem, A. Costa, J. Plant Nutr. 23 (2000) 815–825.
[11] P. Argust, Biol. Trace Elem. Res. 66 (1998) 131–143.
[12] J.L. Parks, M. Edwards, Crit. Rev. Environ. Sci. Technol. 35 (2005) 81–114.
[13] C.C. Vidyasagar, B.M. Muñoz Flores, V.M. Jiménez-Pérez, P.M. Gurubasavaraj, Mater. Today Chem. 11 (2019) 133–155.
[14] H.J. Zhai, B. Kiran, J. Li, L.S. Wang, Nat. Mater 2 (2003) 827–833.
[15] H. Braunschweig, R.D. Dewhurst, K. Kraft, K. Radacki, Angew. Chem. Int. Ed. 48 (2009) 5837–5840.
[16] M.A. Légaré, G. Bélanger-Chabot, R.D. Dewhurst, et al., Science 359 (2018) 896–900.
[17] T. Ogitsu, E. Schwegler, G. Galli, Chem. Rev. 113 (2013) 3425–3449.
[18] H. Braunschweig, R.D. Dewhurst, Dalton Trans. 40 (2011) 549–558.
[19] G. Frenking, N. Fröhlich, Chem. Rev. 100 (2000) 717–774.
[20] Y. Wang, L. Wu, Y. Lin, et al., Phys. Rev. B 92 (2015) 174106.
[21] P. Li, R. Zhou, X.C. Zeng, ACS Appl. Mater. Interfaces 7 (2015) 15607–15617.
[22] J. Akimitsu, T. Muranaka, Phys. C 388-389 (2003) 98–102.
[23] A.T. Lech, C.L. Turner, J. Lei, et al., J. Am. Chem. Soc. 138 (2016) 14398–14408.
[24] T. Muranaka, J. Akimitsu, Phys. C 226 (2011) 385–394.
[25] J.B. Levine, J.B. Betts, J.D. Garrett, S.Q. Guo, J.T. Eng, et al., Acta Mater. 58 (2010) 1530–1535.
[26] P.A. Chen, C.Y. Yang, S.J. Chang, M.H. Lee, N.K. Tang, J. Magn. Magn. Mater. 370 (2014) 45–53.
[27] B. Ganem, J.O. Osby, Chem. Rev. 86 (1986) 763–780.
[28] R.N. Grimes, Science 194 (1976) 709–710.
[29] H.C. Brown, Science 210 (1980) 485–492.
[30] A. Suzuki, Angew. Chem. Int. Ed. 50 (2011) 6722–6737.
[31] R. Paul, P. Buisson, N. Joseph, Ind. Eng. Chem. Res. 44 (1952) 1006–1010.
[32] X. Fan, X. Xiao, L. Chen, et al., J. Mater. Chem. A 1 (2013) 11368–11375.
[33] S. Carenco, D. Portehault, C. Boissière, N. Mézailles, C. Sanchez, Chem. Rev. 113 (2013) 7981–8065.
[34] T.S.R.C. Murthy, J.K. Sonber, K. Sairam, R.D. Bedse, J.K. Chakarvartty, Mater. Today Proc. 3 (2016) 3104–3113.
[35] E. Bykova, A.A. Tsirlin, H. Gou, L. Dubrovinsky, N. Dubrovinskaia, J. Alloy. Compd. 608 (2014) 69–72.
[36] J.M. Venegas, W.P. McDermott, I. Hermans, Acc. Chem. Res. 51 (2018) 2556–2564.
[37] Y. Chen, G. Yu, W. Chen, et al., J. Am. Chem. Soc. 139 (2017) 12370–12373.
[38] M. Wang, X. Qin, K. Jiang, et al., J. Phys. Chem. C 121 (2017) 3416–3423.
[39] N. Wang, A. Xu, P. Ou, et al., Nat. Commun. 12 (2021) 6089.
[40] R. Guo, K. Zhang, S. Ji, Y. Zheng, M. Jin, Chin. Chem. Lett. 32 (2021) 2679–2692.
[41] J.T. Kim, S.H. Hong, X. Bian, et al., Intermetallics 99 (2018) 1–7.
[42] H. Sun, J. Meng, L. Jiao, F. Cheng, J. Chen, Inorg. Chem. Front. 5 (2018) 760–772.
[43] G. Gouget, P. Beaunier, D. Portehault, C. Sanchez, Faraday Discuss. 191 (2016) 511–525.
[44] B. Wang, D.Y. Wang, Z. Cheng, X. Wang, Y.X. Wang, ChemPhysChem 14 (2013) 1245–1255.
[45] S.C. Chien, S. Chattopadhyay, L.C. Chen, S.T. Lin, K.H. Chen, Diam. Relat. Mater. 12 (2003) 1463–1471.
[46] T. Ma, P. Zhu, X. Yu, Chin. Phys. B 30 (2021) 108103.
[47] Q. Li, X. Zou, X. Ai, et al., Adv. Energy Mater. 9 (2019) 1803369.
[48] X. Ai, X. Zou, H. Chen, et al., Angew. Chem. Int. Ed. 59 (2020) 3961–3965.
[49] Z. Li, Z. Xie, H. Chen, et al., Chem. Eng. J. 419 (2021) 129568.
[50] Z. Li, X. Ai, H. Chen, et al., Chem. Commun. 57 (2021) 5075–5078.
[51] K. Deng, T. Ren, Y. Xu, et al., J. Mater. Chem. A 8 (2020) 5595–5600.
[52] F. Guo, Y. Wu, X. Ai, et al., Chem. Commun. 55 (2019) 8627–8630.
[53] Q. Xia, Y. Hu, Y. Wang, et al., Nanoscale 14 (2022) 1264–1270.
[54] A.J. Mannix, Z. Zhang, N.P. Guisinger, B.I. Yakobson, M.C. Hersam, Nat. Nanotechnol. 13 (2018) 444–450.
[55] X. Liu, Y. Jiao, Y. Zheng, S.Z. Qiao, ACS Catal. 10 (2020) 1847–1854.
[56] F. Guo, Y. Wu, H. Chen, et al., Energy Environ. Sci. 12 (2019) 684–692.
[57] T.T.V. Doan, J. Wang, K.C. Poon, et al., Angew. Chem. Int. Ed. 55 (2016) 6842–6847.
[58] D.H. Quiñones, A. Rey, P.M. Álvarez, F.J. Beltrán, G.L. Puma, Appl. Catal. B 178 (2015) 74–81.
[59] E.B. Simsek, Appl. Catal. B 200 (2017) 309–322.
[60] H. Ding, H. Liu, W. Chu, C. Wu, Y. Xie, Chem. Rev. 121 (2021) 13174–13212.
[61] D. He, L. Zhang, D. He, et al., Nat. Commun. 7 (2016) 12362.
[62] S. Jin, ACS Energy Lett. 2 (2017) 1937–1938.
[63] A.L. James, M. Lenka, N. Pandey, et al., Nanoscale 12 (2020) 17121–17131.
[64] T. Chen, C. Foo, S.C.E. Tsang, Chem. Sci. 12 (2021) 517–532.
[65] F. Müller, M. Lessel, S. Grandthyll, et al., Langmuir 29 (2013) 4543–4550.
[66] S.K. Nayak, C.J. Hung, V. Sharma, et al., npj Comput. Mater. 4 (2018) 11.
[67] R. Janisch, C. Elsässer, Phys. Rev. B 67 (2003) 224101.
[68] J. Feng, R.G. Hennig, N.W. Ashcroft, R. Hoffmann, Nature 451 (2008) 445–448.
[69] F. Shao, Z. Yao, Y. Gao, et al., Chin. J. Catal. 42 (2021) 1185–1194.
[70] Y. Niu, X. Huang, Y. Wang, et al., Nat. Commun. 11 (2020) 3324.
[71] I.T. Ellis, E.H. Wolf, G. Jones, Chem. Commun. 53 (2017) 601–604.
[72] L. Zhang, J. Lu, S. Yin, et al., Appl. Catal. B: Environ. 230 (2018) 58–64.
[73] L. Li, Z. Deng, L. Yu, Z. Lin, W. Wang, G. Yang, Nano Energy 27 (2016) 103–113.
[74] C. Lu, P.R. Jothi, T. Thersleff, et al., Nanoscale 12 (2020) 3121–3128.
[75] R. Li, Z. Liu, Q.T. Trinh, et al., Adv. Mater. 33 (2021) 2101536.
[76] Y. Lin, J.W. Connell, Nanoscale 4 (2012) 6908–6939.
[77] M.D. Esrafili, S. Asadollahi, ChemistrySelect 3 (2018) 9181–9188.
[78] P. Joshi, R. Yadav, M. Hara, et al., J. Mater. Chem. A 9 (2021) 9066–9080.
[79] S. Büchele, Z. Chen, E. Fako, et al., Angew. Chem. Int. Ed. 59 (2020) 19639–19644.
[80] J. Zhu, P. Wei, K. Li, et al., ACS Sustain. Chem. Eng. 7 (2019) 660–668.
[81] H. Chen, X. Zou, Inorg. Chem. Front. 7 (2020) 2248–2264.
[82] G. Akopov, M.T. Yeung, R.B. Kaner, Adv. Mater. 29 (2017) 1604506.
[83] H. Park, A. Encinas, J.P. Scheifers, Y. Zhang, B.P.T. Fokwa, Angew. Chem. Int. Ed. 56 (2017) 5575–5578.
[84] P.R. Jothi, Y.M. Zhang, J.P. Scheifers, H. Park, B.P.T. Fokwa, Sustain. Energ. Fuels 1 (2017) 1928–1934.
[85] H. Li, P. Wen, Q. Li, et al., Adv. Energy Mater. 7 (2017) 1700513.
[86] E. Lee, H. Park, H. Joo, B.P.T. Fokwa, Angew. Chem. Int. Ed. 59 (2020) 11774–11778.
[87] X. Guo, S. Lin, J. Gu, et al., Adv. Funct. Mater. 31 (2021) 2008056.
[88] L. Wang, J. Li, X. Zhao, Adv. Mater. Interfaces 6 (2019) 1801690.
[89] Z.H. Pu, T.T. Liu, G.X. Zhang, et al., Small Methods 5 (2021) 2100699.
[90] J. Masa, W. Schuhmann, ChemCatChem 11 (2019) 5842–5854.
[91] D.K. Mann, J. Xu, N.E. Mordvinova, et al., Chem. Sci. 10 (2019) 2796–2804.
[92] R.F. Tian, S.J. Zhao, J.K. Li, et al., J. Mater. Chem. A 9 (2021) 6469–6475.
[93] X. Ma, K. Zhao, Y. Sun, et al., Catal. Sci. Technol. 10 (2020) 2165–2172.

[94] A. Saad, Y. Gao, A. Ramiere, et al., Small 18 (2022) 2201067.
[95] J. Masa, I. Sinev, H. Mistry, et al., Adv. Energy Mater. 7 (2017) 1700381.
[96] X. Ma, J. Wen, S. Zhang, et al., ACS Sustain. Chem. Eng. 5 (2017) 10266–10274.
[97] X. Zheng, B. Zhang, P. De Luna, et al., Nat. Chem. 10 (2018) 149–154.
[98] D.A. Kuznetsov, B. Han, Y. Yu, et al., Joule 2 (2018) 225–244.
[99] W.J. Jiang, S. Niu, T. Tang, et al., Angew. Chem. Int. Ed. 56 (2017) 6572–6577.
[100] J. Li, Y. Liu, H. Chen, et al., Adv. Funct. Mater. 31 (2021) 2101820.
[101] R.J. Toh, H.L. Poh, Z. Sofer, M. Pumera, et al., Chem. Asian J. 8 (2013) 1295–1300.
[102] Y.Y. Chen, Y. Zhang, W.J. Jiang, et al., ACS Nano 10 (2016) 8851–8860.
[103] D. Wang, T. Liu, J. Wang, Z. Wu, Carbon 139 (2018) 845–852.
[104] H. Wang, C. Tsai, D. Kong, Nano Res. 8 (2015) 566–575.
[105] A. Sarapuu, E. Kibena-Põldsepp, M. Borgheib, K. Tammeveski, J. Mater. Chem. A 6 (2018) 776–804.
[106] B. Jiang, X.G. Zhang, K. Jiang, et al., J. Am. Chem. Soc. 140 (2018) 2880–2889.
[107] T.W. Jiang, Y.W. Zhou, X.Y. Ma, et al., ACS Catal. 11 (2021) 840–848.
[108] Y. Zhou, F. Che, M. Liu, et al., Nat. Chem. 10 (2018) 974–980.
[109] Y. Song, J.R.C. Junqueira, N. Sikdar, et al., Angew. Chem. Int. Ed. 60 (2021) 9135–9141.
[110] J. Li, J. Chen, Q. Wang, W.B. Cai, S. Chen, Chem. Mater. 29 (2017) 10060–10067.
[111] F. Li, Q. Tang, Nanoscale 11 (2019) 18769–18778.
[112] K. Chu, Y.P. Liu, Y.H. Cheng, Q.Q. Li, J. Mater. Chem. A 8 (2020) 5200–5208.
[113] X. Yu, P. Han, Z. Wei, L. Huang, Z. Gu, et al., Joule 2 (2018) 1610–1622.
[114] K. Natsui, H. Iwakawa, N. Ikemiya, K. Nakata, Y. Einaga, Chem. Int. Ed. 57 (2018) 2639–2643.
[115] L. Yang, S. Jiang, Y. Zhao, Angew. Chem. Int. Ed. 50 (2011) 7132–7135.
[116] J. Yu, L. Qi, M. Jaroniec, J. Phys. Chem. C 114 (2010) 13118–13125.
[117] I. Tsuji, H. Kato, A. Kudo, Angew. Chem. Int. Ed. 44 (2005) 3565–3568.
[118] K. Maeda, N. Sakamoto, T. Ikeda, et al., Chem. Eur. J. 16 (2010) 7750–7759.
[119] F.N. Sayed, O.D. Jayakumar, R. Sasikala, et al., J. Phys. Chem. C 116 (2012) 12462–12467.
[120] M. Murdoch, G.I.N. Waterhouse, M.A. Nadeem, et al., Nat. Chem. 3 (2011) 489–492.
[121] S. Onsuratoom, T. Puangpetch, S. Chavadej, Chem. Eng. J. 173 (2011) 667–675.
[122] D. Qiao, C. Xu, J. Xu, Catal. Commun. 45 (2014) 44–48.
[123] L. Bao, F. Yang, D. Cheng, et al., Appl. Surf. Sci. 513 (2020) 145767.
[124] Q. Zhu, B. Qiu, M. Du, et al., Ind. Eng. Chem. Res. 57 (2018) 8125–8130.
[125] X. Lu, J. Xie, S.Y. Liu, et al., ACS Sustain. Chem. Eng. 6 (2018) 13140–13150.
[126] L. Jiang, Y. Guo, S. Qi, et al., Dalton Trans. 50 (2021) 17960–17966.
[127] X. Meng, J. Yang, S. Xu, et al., Chem. Eng. J. 410 (2021) 128339.
[128] Q. Fu, Y. Meng, Z. Fang, ACS Appl. Mater. Interfaces 9 (2017) 2469–2476.
[129] S. Back, S. Siahrostami, Nanoscale Adv. 1 (2019) 132–139.
[130] Y. Chen, J. Cai, P. Li, et al., Nano Lett. 20 (2020) 6807–6814.
[131] Q. Li, L. Li, X. Yu, et al., Chem. Eng. J. 399 (2020) 125827.
[132] Q. Li, T. Zhang, X. Yu, et al., Front. Chem. 7 (2019) 674.
[133] C. Deng, W. Li, R. He, W. Shen, M. Li, J. Phys. Chem. 124 (2020) 19530–19537.
[134] J. Zhao, Z. Chen, J. Am. Chem. Soc. 139 (2017) 12480–12487.
[135] S. Tang, Q. Dang, T. Liu, et al., J. Am. Chem. Soc. 142 (2020) 19308–19315.
[136] D.K. Yesudoss, G. Lee, S. Shanmugam, Appl. Catal. B 287 (2021) 119952.
[137] H. Liu, X.H. Zhang, X. Y, et al., Adv. Energy Mater. 10 (2020) 1902521.
[138] M.A. Légaré, G. Bélanger-Chabot, M. Rang, et al., Nat. Chem. 12 (2020) 1076–1080.
[139] Y. Wen, Z. Zhuang, H. Zhu, et al., Adv. Energy Mater. 11 (2021) 2102138.
[140] X. Lv, W. Wei, F. Li, B. Huang, Y. Dai, Nano Lett. 19 (2019) 6391–6399.
[141] H. Yin, L.Y. Gan, P. Wang, J Mater. Chem. A 8 (2020) 3910–3917.
[142] P. Lanzafame, S. Perathoner, G. Centi, S. Gross, E.J.M. Hensen, Catal. Sci. Technol. 7 (2017) 5182–5194.